Fault Status Assessment for Fault Diagnosis of a Multistage Planetary Gear Set Based on Dynamic Simulation and Experimental Analysis

Guoyan Li, Fangyi Li, Dehao Dong, Jianfeng Li, Haohua Liu and Yifan Wang

Abstract This paper aims at extracting and selecting suitable fault features to assess the damage status of planetary gearbox based on simulated and experimental signals. A nonlinear dynamic model of a two-stage planetary gear set is established. For this model, an improved potential energy method is used to calculate the time-varying gear mesh stiffness considering the influence of different crack levels in the sun gear of the second stage. Then, several fault features are provided to assess the crack propagation levels based on the simulated signals. Afterwards, the change percentages of these statistical indicators are compared for evaluating the sensitivity of each fault feature. Finally, the actual vibration data collected from an industrial planetary gearbox with pitting and broken tooth damages are provided to validate the theoretical derivations.

Keywords Multistage compound planetary gear set · Nonlinear dynamic model · Time-varying mesh stiffness · Fault features selection

G. Li · F. Li (✉) · D. Dong · J. Li · H. Liu · Y. Wang
Ministry of Education Key Laboratory of High-Efficiency and Clean Mechanical Manufacture, School of Mechanical Engineering, Shandong University, 250061 Jinan, China
e-mail: lifangyi@sdu.edu.cn

G. Li
e-mail: liguoyan821@qq.com

D. Dong
e-mail: 86189738@qq.com

J. Li
e-mail: ljf@sdu.edu.cn

H. Liu
e-mail: 1115908998@qq.com

Y. Wang
e-mail: wangyifan102007@126.com

R. Setchi et al. (eds.), *Sustainable Design and Manufacturing 2016*,
Smart Innovation, Systems and Technologies 52,
DOI 10.1007/978-3-319-32098-4_57

1 Introduction

Many industrialized countries need to consider the resource shortage and environmental issue. Scrapped machineries still have high salvage value. So, remanufacturing becomes a best solution to deal with these concerns. Planetary gearboxes are widely used in large-scale and complex mechanical equipments, such as wind turbines, helicopters, construction machineries, and etc. However, the damage statuses of recycled gearboxes are complicated and various due to their different service conditions and geometric structures. Therefore, the fault diagnosis of the recycled objects plays a key role in assuring the remanufactured products' quality.

So far, the common fault features can be divided into the time-domain statistical indicators, the frequency spectrum analysis indicators, and the feature parameters specially designed for gear damage assessment [1, 2]. However, the redundant and irrelevant features will increase the computation burden, impact the classification accuracy, and make the model more complex. Thus, selecting best fault features out of all the indicators becomes a new challenge in recent years. Due to the influence of strong environmental noise, the incipient fault signatures are always too weak to be identified. Moreover, the fault forms and levels are various in practice. So, it's difficult to directly evaluate the effectiveness and sensibility of the fault features through the collected signals. Therefore, model-based dynamic analysis and simulations become important methods to evaluate the fault features. The compound and multistage planetary gear sets are common in construction machineries due to the requirement of more compact structures and complex transmissions [3]. So the vibration signal analysis and fault status assessment should consider more complicated factors.

This paper aims at providing a dynamic model to simulate the corresponding dynamic responses of the two-stage planetary gear system. Based on the simulated signals, the effective and sensitive of 11 features for reflecting the fault status are compared. Finally, the theoretical derivations provided in the simulation are validated based on the actual signals including pitting and broken damage information.

2 Nonlinear Dynamic Model of a Two-Stage Planetary Gear Set

The detailed description about the two-stage planetary gear set analyzed in this section has been presented in previous work [3]. The lumped-parameter dynamic model for the gear set is shown in Fig. 1. Only one of the planet branches located at a random spacing angle is shown for simplicity purpose. Each component j is allowed to translate in x and y directions and rotate around the axis based on a fixed absolute coordinate frame, denoted by x_j, y_j and θ_j (j = the center components c, r, s_1, s_2, and the planets $p_i(\dot{p}_i, \bar{p}_i, \hat{p}_i)$). All the components are assumed to be ideal rigid body with the mass m_j and the mass moment of inertia I_j. In the dynamic model, the gear mesh interfaces are modeled by spring-damping structures. The time-varying mesh

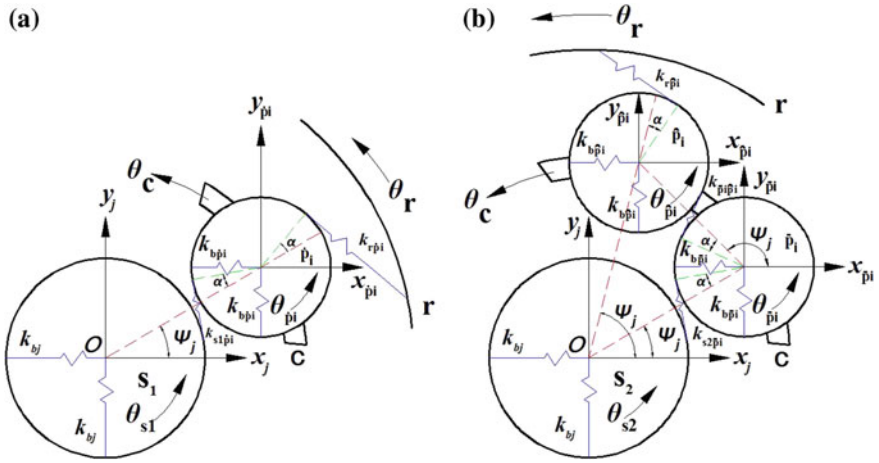

Fig. 1 A lumped-parameter dynamic model for the two-stage planetary gear set

stiffness k_{jpi} is calculated by using improved potential energy method, and the viscous mesh damping coefficient c_{jpi} is set to be proportional to the total mesh stiffness defined as $c_{jpi} = \mu_{jpi} k_{jpi}$ (μ_{jpi} is the scale constant measured in seconds). The linear spring-damping structures are also adopted to represent the bearing supports, where k_{bj} and c_{bj} denote the bearing support stiffness and damping coefficient in radial direction respectively. k_{uj} and c_{uj} are the torsional support stiffness and damping coefficient.

The differential equations for the sun gear, ring gear and planets can be derived as Eqs. (1)–(6) [3]:

$$\begin{cases} m_{s1}\ddot{x}_{s1} - \sum_{i=1}^{N} \sin\varphi_{s1\dot{p}i} F_{s1\dot{p}i} + F_{bs1x} = 0 \\ m_{s1}\ddot{y}_{s1} + \sum_{i=1}^{N} \cos\varphi_{s1\dot{p}i} F_{s1\dot{p}i} + F_{bs1y} = 0 \\ \frac{I_{s1}}{r_{s1}^2}\ddot{u}_{s1} + \sum_{i=1}^{N} F_{s1\dot{p}i} + F_{us1} = 0 \end{cases} \tag{1}$$

$$\begin{cases} m_{s2}\ddot{x}_{s2} - \sum_{i=1}^{N} \sin\varphi_{s2\bar{p}i} F_{s2\bar{p}i} + F_{bs2x} = 0 \\ m_{s2}\ddot{y}_{s2} + \sum_{i=1}^{N} \cos\varphi_{s2\bar{p}i} F_{s2\bar{p}i} + F_{bs2y} = 0 \\ \frac{I_{s2}}{r_{s2}^2}\ddot{u}_{s2} + \sum_{i=1}^{N} F_{s2\bar{p}i} + F_{us2} = \frac{T_{in}}{r_{s2}} \end{cases} \tag{2}$$

$$\begin{cases} m_r\ddot{x}_r + \sum_{i=1}^{N} \sin\varphi_{r\hat{p}i} F_{r\hat{p}i} - \sum_{i=1}^{N} \sin\varphi_{r\dot{p}i} F_{r\dot{p}i} + F_{brx} = 0 \\ m_r\ddot{y}_r - \sum_{i=1}^{N} \cos\varphi_{r\hat{p}i} F_{r\hat{p}i} + \sum_{i=1}^{N} \cos\varphi_{r\dot{p}i} F_{r\dot{p}i} + F_{bry} = 0 \\ \frac{I_r}{r_r^2}\ddot{u}_r - \sum_{i=1}^{N} F_{r\hat{p}i} + \sum_{i=1}^{N} F_{r\dot{p}i} + F_{ur} = 0 \end{cases} \tag{3}$$

$$\begin{cases} m_{\dot{p}i}\ddot{x}_{\dot{p}i} + \sin\varphi_{s1\dot{p}i} F_{s1\dot{p}i} + \sin\varphi_{r\dot{p}i} F_{r\dot{p}i} = 0 \\ m_{\dot{p}i}\ddot{y}_{\dot{p}i} - \cos\varphi_{s1\dot{p}i} F_{s1\dot{p}i} - \cos\varphi_{r\dot{p}i} F_{r\dot{p}i} = 0 \\ \frac{I_{\dot{p}i}}{r_{\dot{p}i}^2}\ddot{u}_{\dot{p}i} + F_{s1\dot{p}i} - F_{r\dot{p}i} = 0 \end{cases} \tag{4}$$

$$\begin{cases} m_{\bar{p}i}\ddot{x}_{\bar{p}i} + \sin\varphi_{\bar{p}i\hat{p}i} F_{\bar{p}i\hat{p}i} + \sin\varphi_{s2\bar{p}i} F_{s2\bar{p}i} = 0 \\ m_{\bar{p}i}\ddot{y}_{\bar{p}i} - \cos\varphi_{\bar{p}i\hat{p}i} F_{\bar{p}i\hat{p}i} - \cos\varphi_{s2\bar{p}i} F_{s2\bar{p}i} = 0 \\ \frac{I_{\bar{p}i}}{r_{\bar{p}i}^2}\ddot{u}_{\bar{p}i} + F_{s2\bar{p}i} - F_{\bar{p}i\hat{p}i} = 0 \end{cases} \tag{5}$$

$$\begin{cases} m_{\hat{p}i}\ddot{x}_{\hat{p}i} - \sin\varphi_{\bar{p}i\hat{p}i} F_{\bar{p}i\hat{p}i} - \sin\varphi_{r\hat{p}i} F_{r\hat{p}i} = 0 \\ m_{\hat{p}i}\ddot{y}_{\hat{p}i} + \cos\varphi_{\bar{p}i\hat{p}i} F_{\bar{p}i\hat{p}i} + \cos\varphi_{r\hat{p}i} F_{r\hat{p}i} = 0 \\ \frac{I_{\hat{p}i}}{r_{\hat{p}i}^2}\ddot{u}_{\hat{p}i} - F_{\bar{p}i\hat{p}i} + F_{r\hat{p}i} = 0 \end{cases} \tag{6}$$

in these equations, the rotational displacement $u_j = r_j\theta_j$ is defined in place of θ_j, where the parameter r_j is the base radius of each gear, and r_c represents the radius from the carrier center to the planet center. F_{jpi} is the dynamic gear mesh force. F_{bjx}, F_{bjy} and F_{uj} represent the bearing forces in x, y and u directions, respectively. δ_{jpi} is the relative gear mesh displacements along the line of action of stage n, and the detailed derivation is provided in Ref. [3].

The mesh stiffness calculation model described in this section is based on the works in Ref. [4–6]. The gear was simplified as the cantilever beam on the root circle. And the improved energy method was used to analyze the time-varying mesh stiffness, which was assumed to include four components: Hertzian energy u_h, bending energy u_b, shear energy u_s and axial compressive energy u_a. The MATLAB programs are used to obtain the total mesh stiffness. Figure 2 shows the mesh stiffness of a sun-planet mesh pair in the second stage as a function of rotation angle of the sun gear. The mesh duration is from the crack sun gear starting to mesh to the ending of mesh. For the perfect sun-planet mesh pair, the mean mesh stiffness is 1.783×10^9 N/m. For local damage case, we assume that a crack starts from the root of sun gear and propagates with an increment of 10 % (the total crack length is set to be 9.42 mm), it's observed that the mean mesh stiffness becomes lower due to the crack. With respect to crack level 10, 20, 30, 40, 50, 60, 70 %, the corresponding mean mesh stiffness are 1.672×10^9, 1.564×10^9, 1.463×10^9, 1.351×10^9, 1.234×10^9, 1.119×10^9, 9.889×10^8 N/m. The reduction will induce to the obvious changes in dynamic responses of the gear set.

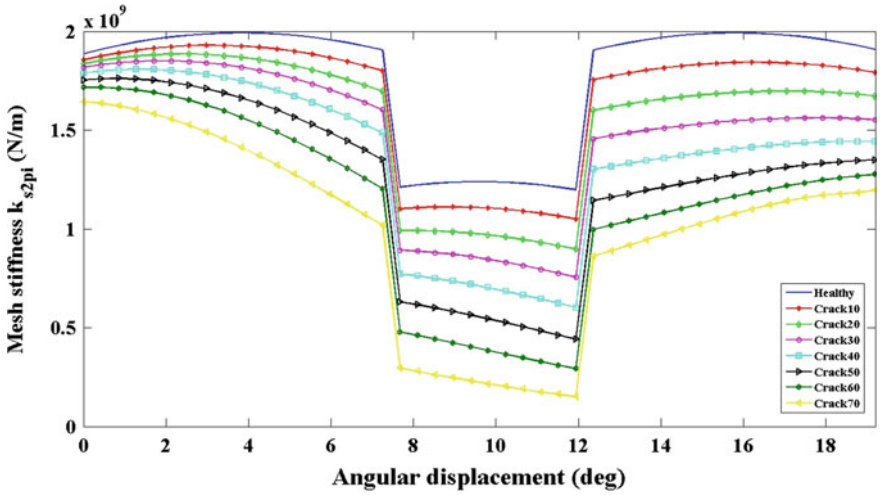

Fig. 2 Total mesh stiffness of the sun-planet mesh pair in the second stage versus angular displacement of sun gear with different crack levels

3 Fault Features Analysis and Crack Level Assessment Based on Dynamic Simulation

In this section, the main parameters used in the simulation are provided in Ref. [3]. And MATLAB's ode15s function is used to solve the equations of motion derived in Sect. 2. The sample frequency and duration time are set to be 5120 Hz and 2 s, respectively. As described above, a crack exists on the sun gear s_2, and propagates from 0 % (the healthy gear set) to 70 % (close to a sudden broken) with an increment rate of 10 %.

In order to focus on the crack status of the sun gear, only the simulated signals of sun gear s_2 are presented in time domain analysis. Figures 3, 4, 5 and 6 show the dynamic responses of the sun gear s_2 in time domain and the corresponding frequency spectra of the system when the crack levels are 0, 30, 50 and 70 %, respectively. For the healthy gear set, the periodic impulses caused by time-varying mesh stiffness are observed in time domain, and the time interval is 0.0055 s. The corresponding spectrum consists of the fundamental meshing frequency of the first stage ($f_1 = 168\,\text{Hz}$), the fundamental meshing frequency of the second stage ($f_2 = 182\,\text{Hz}$), and their harmonics ($kf_1, kf_2(k = 1, 2, \ldots)$). When the cracked sun gear s_2 is in mesh, some other obvious shocks appear in the vibration signals at an impulse period of 0.055 s. And more spectrum peaks appear as sidebands around the frequency components at the frequency of $kf_2 \pm mf_{s2}(k = 1, 2, \ldots, m = 1, 2, \ldots f_{s2} = 18.2\,\text{Hz})$ due to the multiplicative modulation effects caused by the damaged sun gear. As the crack propagates, the amplitudes of these shocks become stronger both in time domain and frequency domain.

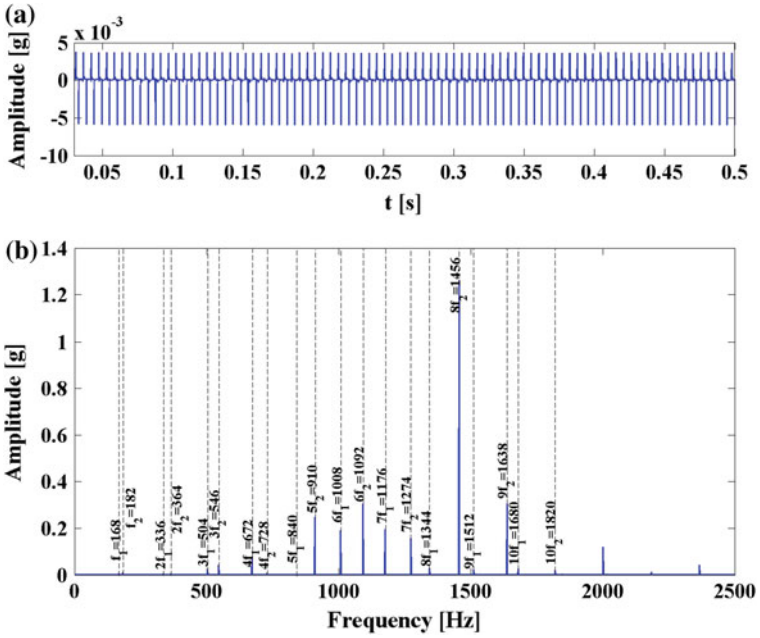

Fig. 3 **a** Dynamic response of the sun gear s_2 in time domain. **b** Frequency spectrum of the system for the healthy gear set

In this section, 11 fault features are selected to assess the crack status as listed in Table 1 [1, 2]. The key is to find out which features are more sensitive to the crack propagation and can be selected to better describe the fault status. To make all the indicators comparable, the change percentage related to the healthy indicators $I_{pj}(j = \mathrm{F1}, \mathrm{F2}, \mathrm{F3}, \ldots, \mathrm{F11})$ are derived as [7–9]:

$$I_{pj} = \frac{I_{\mathrm{damage}j} - I_{\mathrm{healthy}j}}{I_{\mathrm{healthy}j}} \times 100\% \tag{7}$$

in the equation, $I_{\mathrm{damage}j}$ represents the indicator value in the damaged case, and $I_{\mathrm{healthy}j}$ is the indicator value in the healthy case.

Figure 7 shows the calculated results with respect to the crack levels in percentage. The Shape indicator almost has no response to the crack propagation, so it cannot be considered as an effective indicator of fault status. Both in time domain and frequency domain, the RMS and σ have a similar change trend, but the change percentages of these indicators are lower than 30 % even the crack level reaches to 70 %, so they are not sensitive to the crack levels. The performance of the mean frequency is a bit better, and the change percentage is about 56 % related to 70 % crack level. The Crest indicator, Clearance indicator and Impulse indicator keep

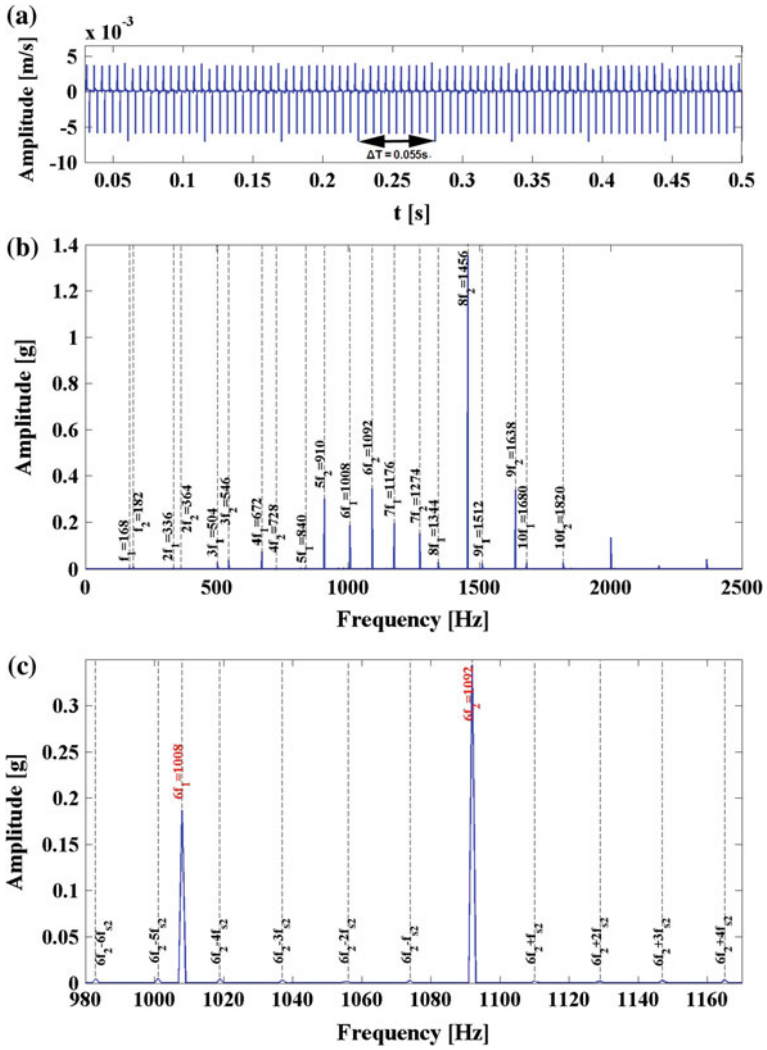

Fig. 4 **a** Dynamic response of the sun gear s_2 in time domain. **b** Frequency spectrum of the system, **c** Enlarged frequency spectrum for the gear set with 30 % crack level

steady increasing pattern as crack propagates, while the Kurtosis and Skewness exhibit a sharp increasing trend when the crack level reaches to 50 %, and the Kurtosis is more sensitive to the severe crack damages. For the slight crack damages ranging from 0 to 30 %, the Crest indicator, Clearance indicator and Impulse indicator show obvious increasing trends, and the Impulse indicator stands out to be the best indicator, but the Kurtosis and Skewness perform bad. So it can be

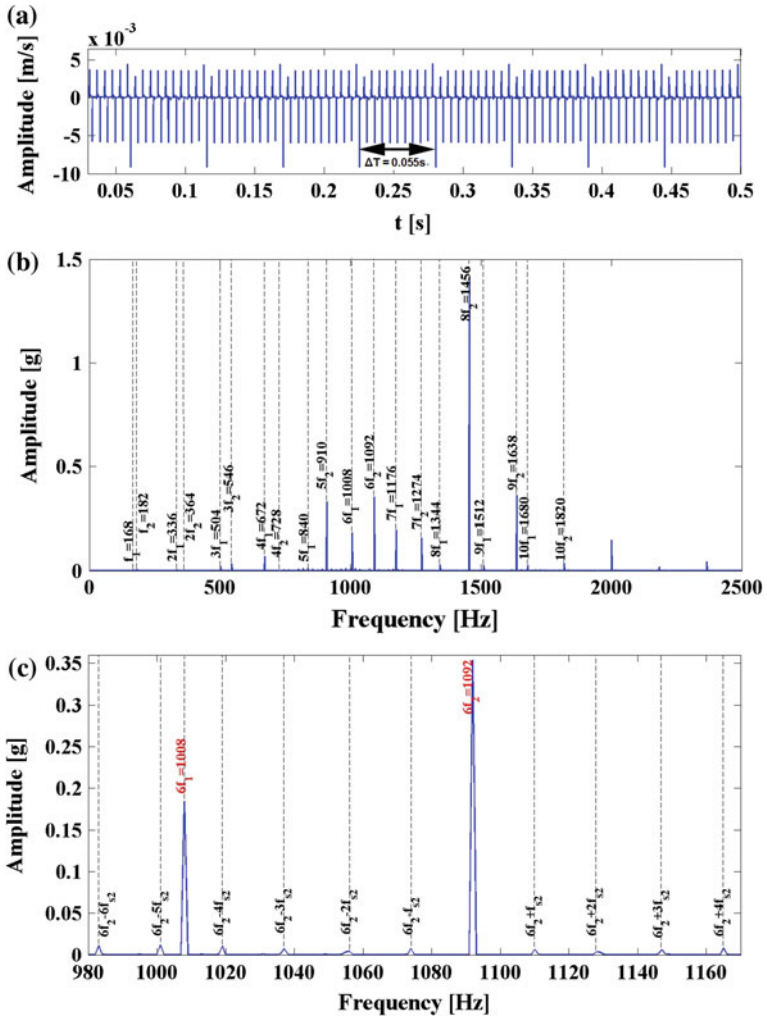

Fig. 5 **a** Dynamic response of the sun gear s_2 in time domain. **b** Frequency spectrum of the system. **c** Enlarged frequency spectrum for the gear set with 50 % crack level

concluded that Crest indicator, Clearance indicator, Impulse indicator and Kurtosis can provide useful information for damage assessment, and Impulse indicator is more sensitive to the early stage faults, while the Kurtosis is more effective when the faults become severe.

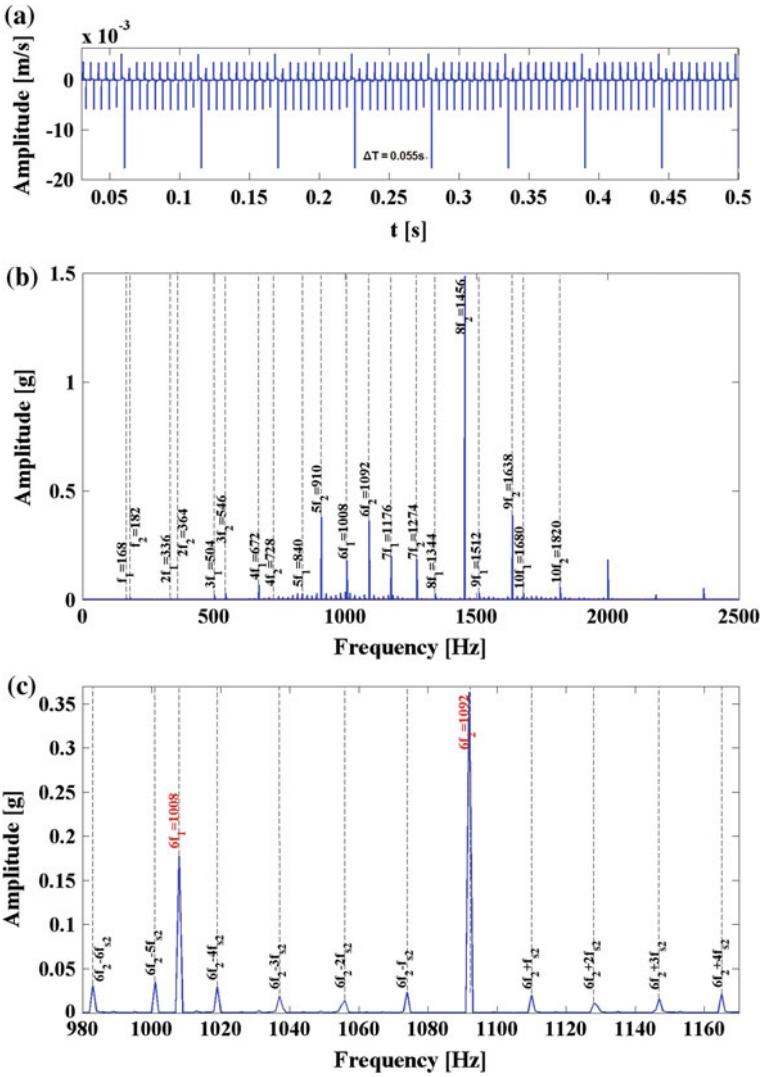

Fig. 6 **a** Dynamic response of the sun gear s_2 in time domain. **b** Frequency spectrum of the system. **c** Enlarged frequency spectrum for the gear set with 70 % crack level

4 Experimental Results

The vibration based experiments have been done on a planetary gearbox test rig, as shown in Fig. 8. The KD1002S three-axis accelerometer is mounted on the test gearbox casing to measure the signals, and the data are recorded by CRAS signal acquire analysis system. The test gearbox is an industrial SD16 planetary gearbox,

Table 1 Definitions of the 11 fault features

	Fault features		Fault features
1	Root mean square	7	Shape indicator
2	Standard deviation	8	Impulse indicator
3	Skewness	9	Mean frequency
4	Kurtosis	10	Root mean square frequency
5	Crest indicator	11	Standard deviation frequency
6	Clearance indicator		

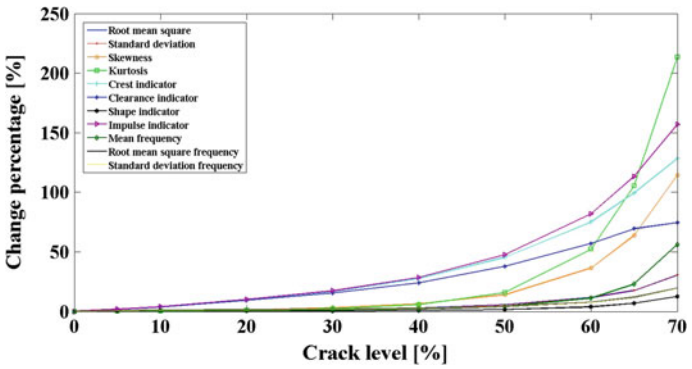

Fig. 7 Comparison among fault features with respect to the crack levels in percentage

as shown in Fig. 9 a, and the system parameters of the second row gear series of this gearbox are the same as the gear model parameter used in the simulation.

To obtain the signal samples, a new sun gear, a pitted sun gear (see Fig. 9b) and a broken sun gear (see Fig. 9c) were considered in the experiments. The vibration signals collected from the new planetary gearbox was considered as baseline level. Then, we mounted the naturally pitted sun gear to replace the perfect sun gear in the second stage to obtain the slight level signals, whereas all the others are normal during the experiment. Similarly, we used a broken sun gear in the second stage to get the severe level signals. During the experiments, the drive motor speed maintained 700 rpm. We considered four load conditions of the load motor: no-load, 200, 600 and 1000 Nm. A 36 s span data was recorded with a sampling frequency of 5120 Hz under each working condition. The same procedures were repeated until three cases were conducted. Each 36 s-long signal was divided into 18 equally time records, so we get 72 signal samples for each damage case under four loading conditions. Figure 10 gives an example of signal samples for each case under the 1000 Nm load condition, respectively.

The change percentages of kurtosis, crest indicator, clearance indicator and impulse indicator selected in the simulation are calculated directly based on each experimental signal sample, as shown in Fig. 11. It can be observed that the mean value of all these features become higher as the damage status becomes worse, so

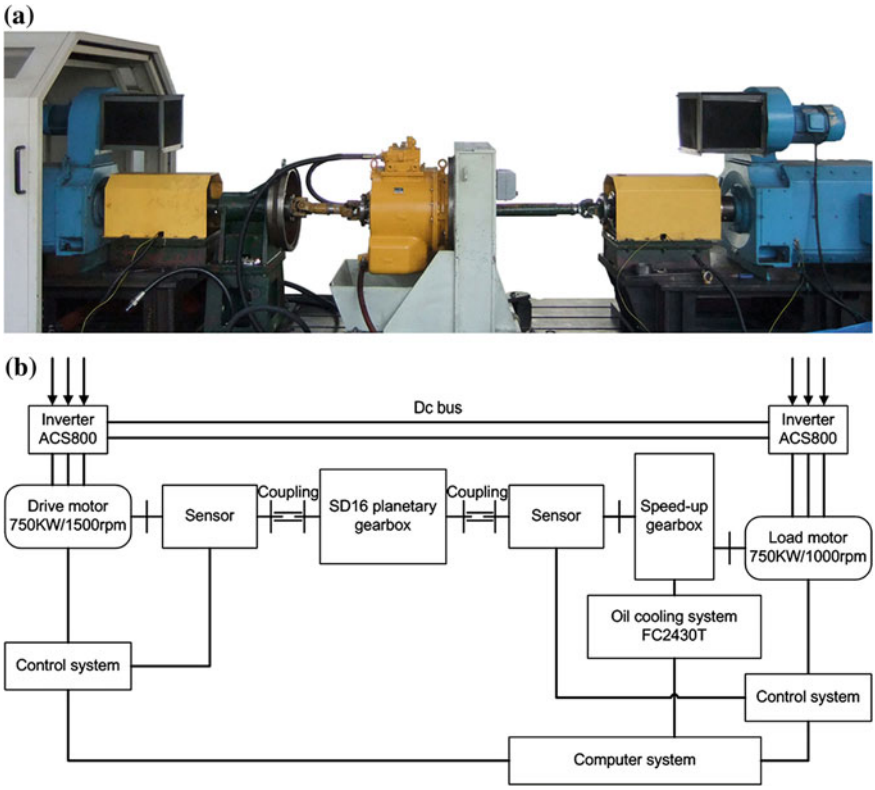

Fig. 8 **a** Planetary gearbox test rig. **b** Structure diagram of the test rig

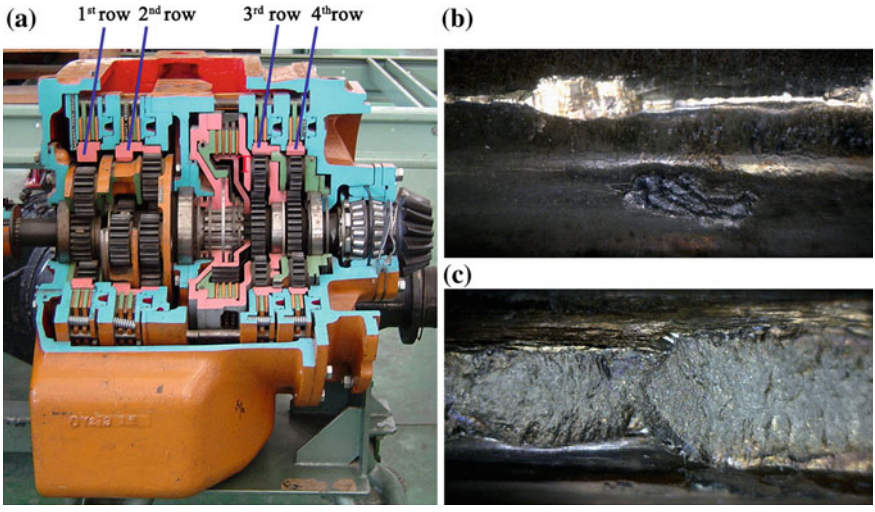

Fig. 9 **a** SD16 planetary gearbox. **b** Pitted sun gear s_2. **c** Sun gear s_2 with broken tooth

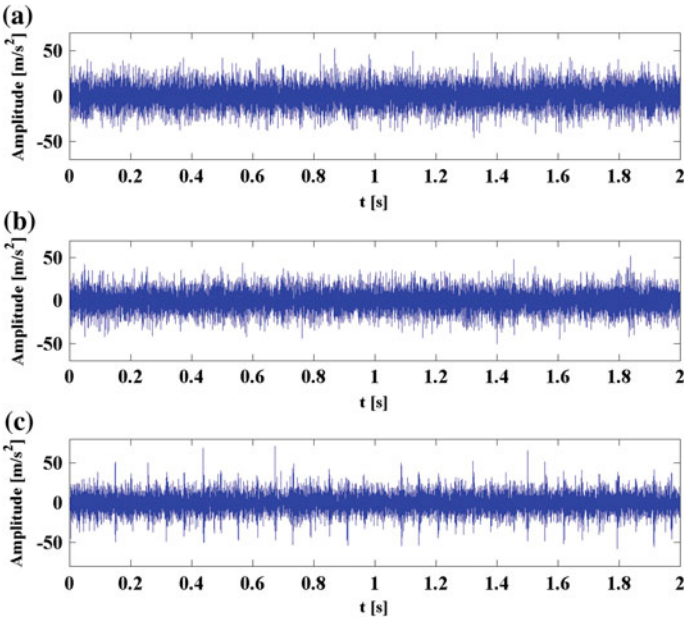

Fig. 10 Typical signal samples **a** new gearbox case, **b** pitted sun gear case, **c** broken sun gear case under 1000 Nm load condition

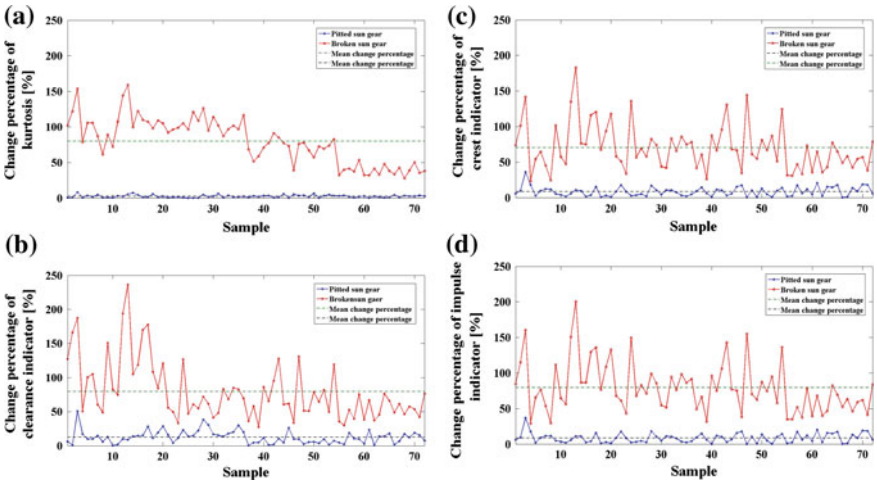

Fig. 11 Assessment results of **a** Kurtosis. **b** Crest indicator. **c** Clearance indicator. **d** Impulse indicator

they can effectively distinguish the fault samples for different damage severity. However, the Crest indicator, Clearance indicator and Impulse indicator are more sensitive to reflect the damage in their early stage than Kurtosis. All the features fluctuate with the change of work conditions.

5 Conclusions

In this paper, a nonlinear dynamic model of a two-stage planetary gear set considering the time-varying mesh stiffness has been established. A crack propagating alone a line is assumed to exist on the sun gear in the second stage, and the corresponding vibration signals are obtained. Several fault features are investigated to evaluate the crack status based on the dynamic simulated signals. It suggests that the kurtosis, crest indicator, clearance indicator and impulse indicator are more effective features for fault status assessment, and all keep increasing pattern as crack propagates. But the crest indicator, clearance indicator and impulse indicator are more sensitive to the early stage faults, while the kurtosis is more sensitive when the faults become severe. The actual test signal samples acquired from the experimental system are used to demonstrate the effectiveness of the proposed fault features for the different gear faults. It suggests that the kurtosis, crest indicator, clearance indicator and impulse indicator can absolutely distinguish the different fault status, and keep increasing trend as the fault becomes severe.

Acknowledgments This research is supported by the National High Technology Research and Development Program of China (No. 2013AA040204).

References

1. Liu, Z.L., Qu, J., Zuo, M.J., Xu, H.B.: Fault level diagnosis for planetary gearboxes using hybrid kernel feature selection and kernel fisher discriminant analysis. Int. J. Adv. Manuf. Technol. **67**, 1217–1230 (2013)
2. Zuo, M.J., Li, W., Fan, X.F.: Statistical methods for low speed planetary gearbox monitoring. Technical report, Department of Mechanical Engineering, University of Alberta, Edmonton (2005)
3. Li, G.Y., Li, F.Y., Wang, Y.F., Dong, D.H.: Fault diagnosis for a multistage planetary gear set using model-based simulation and experimental investigation. Shock Vibr. **2016**, 1–19 (2016)
4. Liang, X.H., Zuo, M.J., Patel, T.H.: Evaluating the time-varying mesh stiffness of a planetary gear set using the potential energy method. Proc. Inst. Mech. Eng. C-J. Mech. **228**, 535–547 (2014)
5. Liang, X.H., Zuo, M.J., Pandey, M.: Analytically evaluating the influence of crack on the mesh stiffness of a planetary gear set. Mech. Mach. Theor. **76**, 20–38 (2014)
6. Wan, Z.G., Cao, H.R., Zi, Y.Y., He, W.P., He, Z.J.: An improved time-varying mesh stiffness algorithm and dynamic modeling of gear-rotor system with tooth root crack. Eng. Fail. Anal. **42**, 157–177 (2014)

7. Wu, S.Y.: Dynamic simulation and estimation of fault growth. M.Sc. Thesis, Department of Mechanical Engineering, University of Alberta Edmonton, Alberta, Canada (2007)
8. Wu, S.Y., Zuo, M.J., Parey, A.: Simulation of spur gear dynamics and estimation of fault growth. J. Sound Vib. **317**, 608–624 (2008)
9. Tian, Z.G., Zuo, M.J., Wu, S.Y.: Crack propagation assessment for spur gears using model-based analysis and simulation. J. Intell. Manuf. **23**, 239–253 (2012)